Chapter V.E Magnetic and Electric Field Configuration

1. Static Fields

a. Specifications

The neutron EDM measurement requires static magnetic and electric fields surrounding the two target cells that contain the superfluid ^{4}He and the ensemble of polarized neutron and ^{3}He atoms. The applied static magnetic field, B_0, is chosen to be about 1 mG resulting in a precession of the magnetic moments of both neutrons and ^{3}He nuclei at about 3 Hz. The static electric field, E_0, should be as strong as possible, consistent with stable operation, to give the largest possible shift of the precession frequency relative to that generated by B_0. The magnetic field should be uniform to 0.1% averaged over each cell volume with a time stability of one part in 10^6 over the period of the precession. The electric field requirement is 1% uniformity over the cell volume and < 1% shift over the ~500 sec measurement period. The basis for these requirements and a specification for E·B is analyzed in the systematic error discussion in Section V.H and is worked out in Ref. 1.

b. Geometry

In the current design for the target volume (see Fig. V.E.1, and for construction details, section V.G), a single HV electrode is flanked by two parallel ground plates that provide equal and opposite electric fields over the two cell volumes. The static magnetic field is generated by a Cos Θ coil cylindrical magnet, which gives an iron-free configuration and a sufficiently uniform magnetic field. The design also includes a superconducting shield around the target region to exclude external fields. It is planned that the volume within the superconducting shield will be filled with superfluid ^{4}He held at a temperature of ~300 mK. Here the ^{3}He, with nominal fractional density, X ~ 10^{-7}, will quickly absorb any UCN created.
The geometry of the electrodes and the magnet coil has to be optimized to achieve the required field uniformity over the two cells. Penetrations through both the superconducting shield and the Cos Θ coil are required to bring in various leads:

a) current leads to the cos Θ coil,
b) the HV and ground leads to the electrodes,
c) SQUID leads,
d) ^{4}He / ^{3}He fill tubes, and
e) light pipes that transport scintillation light from the cell walls to the photomultiplier tubes.

The impact of these penetrations on field uniformity has to be evaluated.

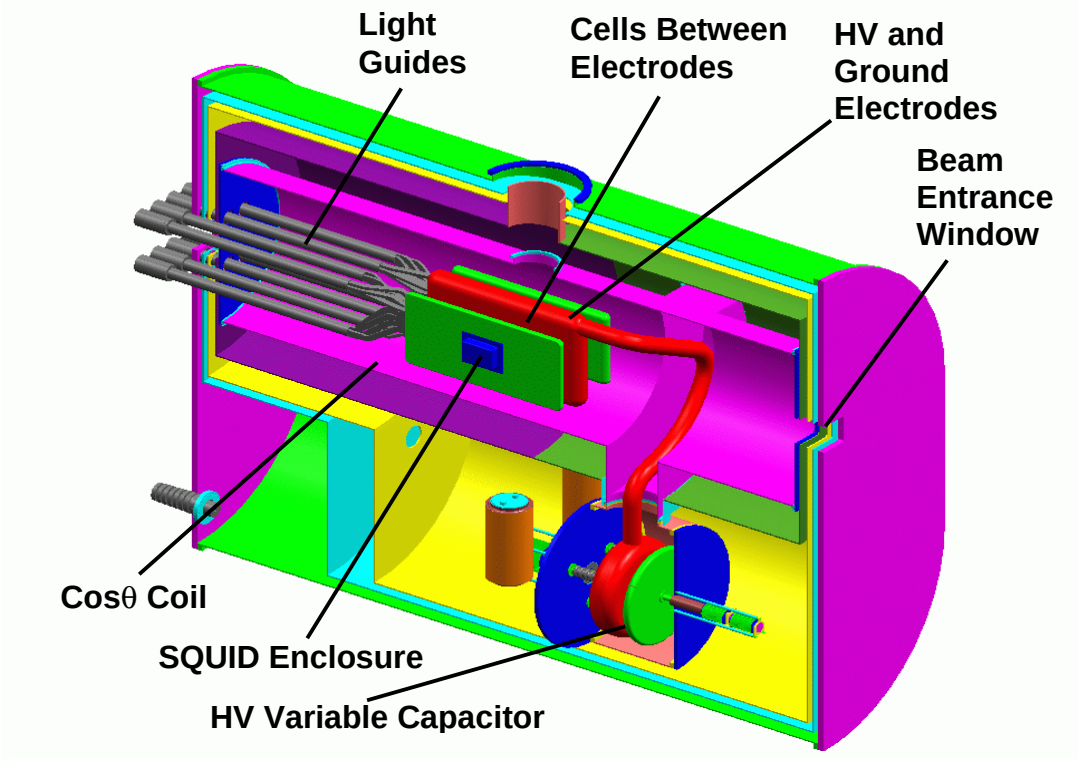

Fig. V.E.1 Design features of the central part of the apparatus including the two neutron / ^{3}He cells and the surrounding static electric field electrodes and the magnetic field Cos Θ coil.

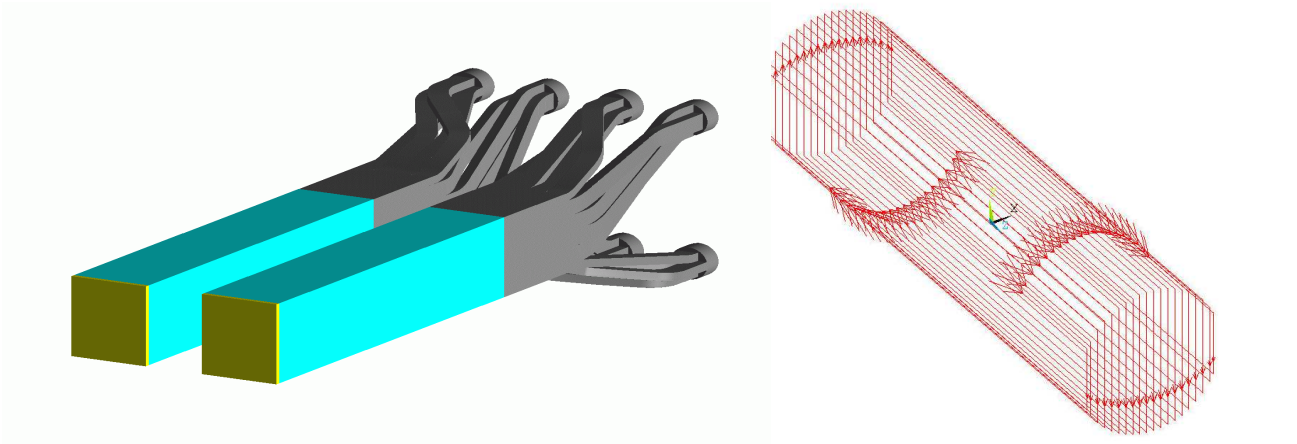

a) b)

Fig V.E.2 a) design of the two cell system, cell volume ~ 4 l. each. The two matching neutron guides are 10 cm x 10 cm (see Section V.A). b) design of the Cos Θ coil cylindrical magnet, R_C = 35 cm, L_C = 200 cm.

The layout of the two cell geometry and the magnetic field coil are shown in Fig V.E.2. Details of the neutron trap design, shown in Fig V.E.2 a**,** are discussed in Section V.C of this proposal. The simulation studies described below lead to the specific geometry for the cells, electrodes, magnetic coil, and superconducting shield listed in Table V.E.1.

Table V.E.1
Nominal Design Parameters
(see text for definition of coordinate system)

Cell(Lucite)	Interior Size:	l_x = 7.6 cm	l_y = 10.2 cm	l_z = 50.0 cm
	Lucite wall thickness 1.3 cm embedded in electrode surface			
Electrodes	Size:	Gap_x = 7.6 cm	L_y = 24.8 cm (gnd) = 29.8 cm (HV)	L_z = 76.5 cm
	Thickness:	ground plate	HV plate	ground plate
	Δx =	5 cm	10 cm	5 cm
Coil (at ground potential)		Radius R_C = 35 cm	Length L_C = 200 cm	
		20 loops, 2.5 cm spacing, end loops at 1.25 cm spacing		
Super-Conducting Shield		Radius R_S = 45 cm	Length L_S = 210 cm	
		penetration = 20 cm diam.		

c. Simulation Studies

In order to study the relation of field uniformity to geometry, a series of electric and magnetic field simulation studies [2] were performed using the ANSYS 5.7 Finite Element Modeling Code. A 2-D model was used for the E field and a 3-D model for the B field.

In the following discussion, the z axis is along the horizontal neutron beam direction and the x axis is along the parallel static magnetic and electric fields in the horizontal plane. The y axis is in the vertical direction. The origin was placed at the geometric center of the HV plane, and because of the reflection symmetry, the uniformity of B_o was tested only in one octant ($x>0$, $y>0$, $z>0$) of the overall volume. The B_o field was evaluated over the eight corners of a rectangular test volume in the above octant. Deviations of the E_o field were evaluated over a nine point grid within the cell in the x-y plane (at $z = 0$). Many field configurations were studied; one good solution for the E_o and B_o fields is shown in Fig V.E.3 and Fig V.E.4 and for the test plane/volume in Fig V.E.5, as discussed below. These results correspond to the design parameters shown in Table V.E.1.

c.1 Electric Field

The electrostatic analysis used 2D static models, with fixed voltage boundary conditions based on the three electrodes, and the volume containing the LHe (assumed to be at ground potential). A rectangular Lucite double cell, Fig V.E.2.a, was adopted with the Lucite walls recessed into the HV and ground electrodes. The dielectric constant of Lucite [3] is taken to be $\varepsilon = 3.0\ \varepsilon_o$ (correct for a temperature of -12 C, however it is not known for 300 mK.) The dielectric constant of liquid ^{4}He is $\varepsilon = 1.05\ \varepsilon_o$ [3]. The distribution of electric field strength is shown in Fig.V.E.3 for a nominal HV of 100 kV applied to the center electrode (13.16 kV/cm in the cell and less in the Lucite). The maximum E field is at the edge of the HV plate, not in the target cell, and reaches 18.5 kV/cm in this example. The uniformity of the electric field for this choice of conditions, Table V.E.1, is shown over the test volume in Fig V.E.5.a.

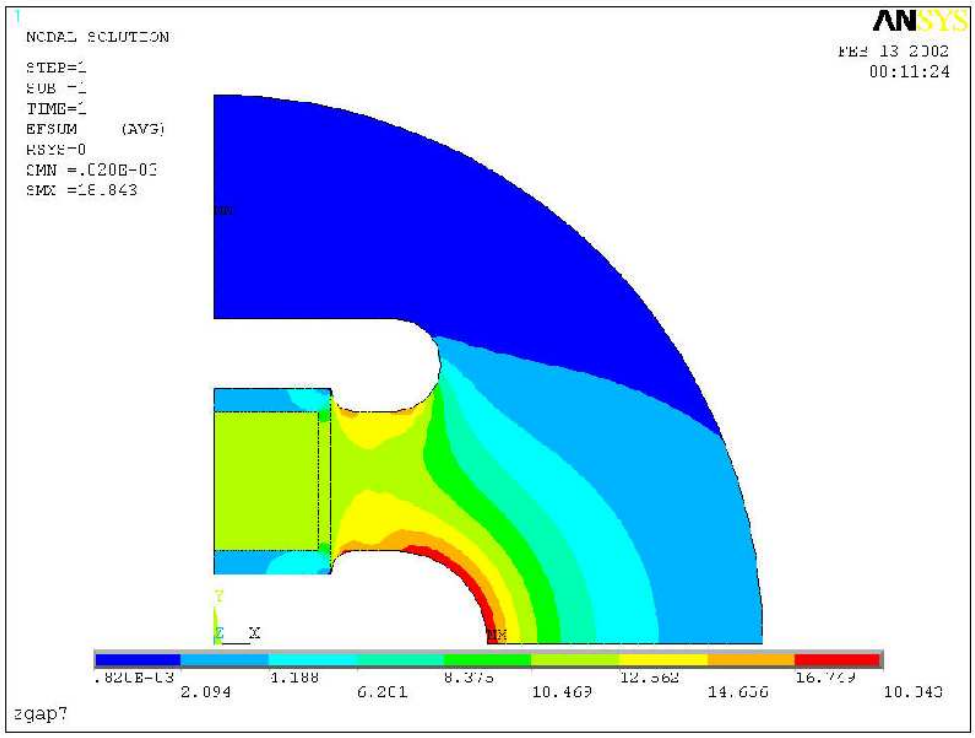

Fig V.E.3 Distribution of electric field strength for the reference design of Table V.E.1.

c.2 Magnetic Field

The magnetic field calculation was based on an array of 20 coils (with uniform current and a 2.5-cm spacing) in a cylindrical geometry as shown in Fig. V.E.2.b. In the current design, Table V.E.1, the two smallest area coils were shifted to a 1.25-cm spacing. A calculated profile of the B_X field component, in the octant x>0, y>0, z>0, is shown in Fig. V.E.4. This

profile is strongly influenced by the radius and length of the superconducting shield. The uniformity of the static magnetic field over the test volume is shown in Fig V.E.5.b.

c.3 Penetrations

To minimize the impact of the HV connection from the variable capacitor to the HV electrode, only nonmagnetic materials should be used. The connection can penetrate the magnetic field coil by entering parallel to the x axis through the opening in the smallest coil. However, this connection must also penetrate the superconducting shield. Since the magnetic field is very sensitive to the placement of this shield, it was critical to simulate the impact of this penetration. A penetration in the shield (20 cm diam.) has been included in the simulation results discussed below, Figs V.E.5 a and b, and can be seen in Fig V.E.4. (In Fig. V.E.4 the penetration is shown on top, but it is actually on the bottom as seen in Fig. V.E.1.) As shown in Fig. V.E.1, the acrylic light pipes from the cells emerge between the layers of the magnet coil and penetrate through the superconducting shield wall. The latter penetrations have not been included in this simulation. The light pipe design must accommodate the sharp temperature changes and minimize the heat load on the cells as discussed in section V. C.

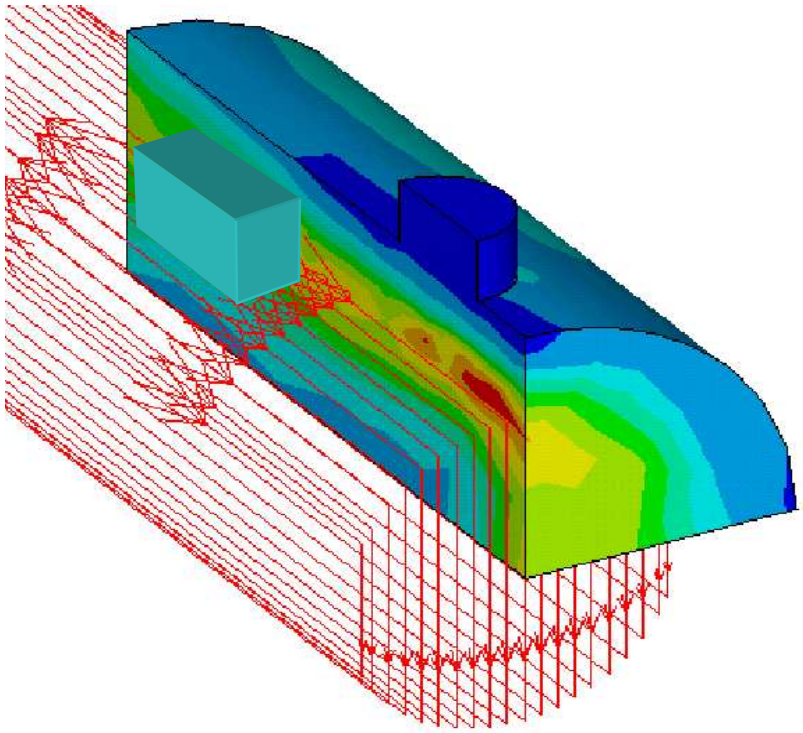

Fig V.E.4 Distribution of magnetic field strength for the reference design of Table V.E.1. The outer cylinder is the superconducting shield with the penetration as shown. The aqua colored rectangle represents the fiducial volume.

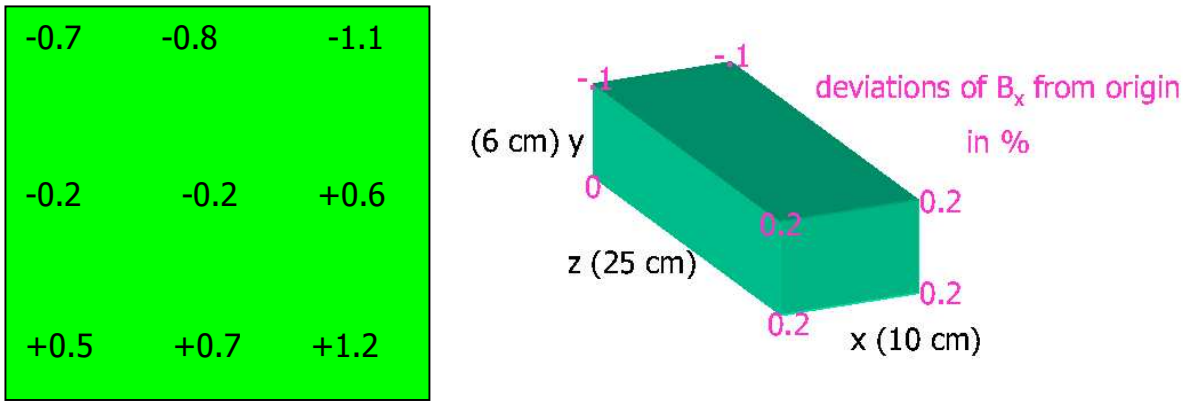

a) Electric field test plane (at z = 0) **b) Magnetic field test volume**

Fig V.E.5 Simulation results for tests of uniformity for the static a) electric and b) magnetic fields. The deviations are in units of %.

d. Results

Many variations in the geometric parameters were studied. Table V.E.1 summarizes the current optimum choice including the effects of the penetration through the superconducting shield.

The corresponding electric field distribution and test plane results, shown in Figs. V.E.3 and V.E.5.a, indicate that the E_o field is uniform over the z = 0 plane of the cell to a rms average value of 0.7%. The maximum electric field that must be sustained, is 1.4 times larger than that in the cell and occurs at the edge of the HV electrode.
The uniformity of the B field distribution is shown in Fig V.E.4 and for the test volume is shown in Fig. V.E.5.b**.** This corresponds to volume averaged rms deviation of 0.15%. These results include the effects of a penetration of the superconducting shield as discussed above.

In conclusion, the design of Table V.E.1 meets the uniformity goals for the static E_o and B_o fields adopted for this neutron EDM experiment. Although this design is expected to be further optimized, this study provides an existence proof that the design goals can be met.

Time stability in the E and B fields is crucial to the success of the measurement. The requirement for the E field is <1.0% shift over the ~500 sec of the measurement. This is discussed in sections V.G and V.H and corresponds to a 1-nA leakage current. This has been achieved in other EDM experiments at higher temperatures. Here operation at 300 mK should improve on this performance measure. Regarding the time stability of the magnetic field, the 1 mG B field generates a precession frequency of 3.0 Hz. The precession frequency shift from the neutron EDM is of the order of ~ 3 μ Hz. Thus the B field must be stable to one part in 10^{-6} over one period of the precession (~ 0.3 sec) or about 10^{-9} G. Typically the coil

requires about 1 mG per mA so a current stability of 1 nA is required. This can be achieved with modern high performance operational amplifiers.

The maximum electric field achievable in this liquid ^{4}He environment is expected to be over 10 kV/mm when liquid ^{4}He is used as the insulating medium. After a search of the literature, we conclude that knowledge of the maximum field value will have to come from a direct measurement. (Information obtained from the literature for the breakdown voltage for liquid ^{4}He is discussed in the V.E Appendix at the end of this section.) A test setup is being built to directly determine the practical limitations of this electric field strength and to investigate long term and short term stability issues. For the B_0 field, the critical issue is the overall uniformity requirement. The B field calculations suggest that the goal of 0.1% can be achieved over cell volumes of 3-5 liters each.

2. Kerr Effect-based Measurement of the Electric field

In order to monitor and control the electric field applied to the target cells, a method based on measuring the Kerr effect with optical polarimetry is being developed.
The Kerr effect is the appearance of uniaxial anisotropy in an initially isotropic medium induced by an applied external electric field $\vec{E}_0$. The optical axis of the induced anisotropy is oriented along the direction of $\vec{E}_0$, and the magnitude of the effect is proportional to E_0^2. The induced anisotropy of the medium results in the electric field dependence of the refractive index (linear birefringence):

$$\Delta n = n_{ll} - n_{\perp} = K\lambda E_0^2 \qquad \text{(V.E.1)}$$

where n_{ll} denotes refractive index for light with linear polarization direction parallel to $\vec{E}_0$ and $n_{\perp}$ - perpendicular to it, λ is the wavelength of the light in vacuum, and K is the Kerr constant of the medium.
Due to the difference between n_{ll} and $n_{\perp}$, an initial linear polarization (with polarization axis directed neither along, nor perpendicular to the applied electric field) of the light passing through the medium, transforms to an elliptical polarization. For input light linearly polarized at 45º to the anisotropy axis, the corresponding ellipticity is

$$\varepsilon = \frac{\pi}{\lambda} l\Delta n = \pi K l E_0^2 \qquad \text{(V.E.2)}$$

where l is the path length in the medium. The Kerr effect has very low inertia. The corresponding relaxation time is ~10^{-11} – 10^{-12} sec providing a possibility for very fast measurement of electric field variations.

A possible experimental arrangement for measuring ellipticity of the light, is the so-called "circular analyzer" [4], which consists of a quarter-wave (λ/4) plate and a polarizing beam splitter (analyzer) with its axis oriented at 45º to the fast axis of the λ/4 -plate. A circular analyzer in this arrangement, is sensitive to the outgoing light ellipticity and insensitive to the angle of rotation of the polarization. Reviews of precision polarimetry techniques and discussions of limiting factors can be found in Refs. 5 and 6.

A circular analyzer based experimental arrangement is shown in Fig. V.E.6. The Kerr medium is placed between the polarizer and the analyzer. The electric field is oriented at 45º with respect to the axis of the polarizer. The normalized difference in the light intensities, I_1 and I_2 (in photons per second), in the two arms of the analyzer, is a measure of the electric-field-induced ellipticity of the outgoing light:

$$\varepsilon = \frac{I_1 - I_2}{2(I_1 + I_2)} \qquad \text{(V.E.3)}$$

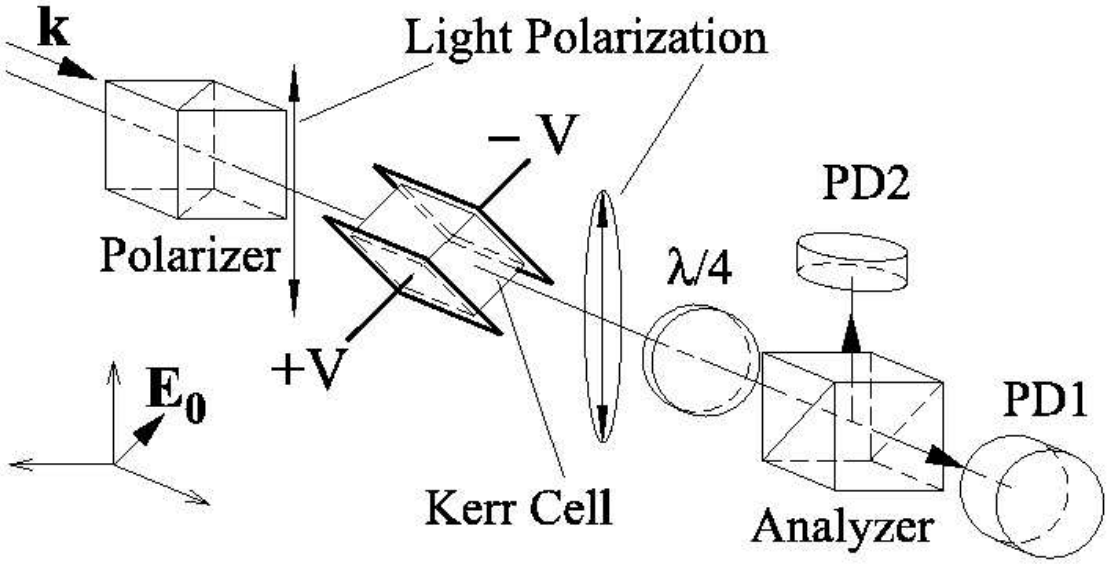

Figure V.E.6. Schematic diagram of an experimental arrangement to measure the Kerr effect.

The shot-noise-limited sensitivity of the polarimeter shown in Fig. V.E.6 is (see, e.g. Ref. 6):

$$\delta\varepsilon \approx \frac{1}{2\sqrt{(I_1 + I_2)T}} \qquad \text{(V.E.4)}$$

where T is the data accumulation time. For input light power of a few milliwatts, $\delta\varepsilon \sim 10^{-8}$ rad/s$^{1/2}$. According to Eq. V.E.2, ε is also a measure of the applied electric field. An attractive property of such measurements is the absence of any kind of electric field "probe" or access devices (electrical, mechanical, etc.), except for input/output light access, which can be achieved using simple fiber coupling.

In the framework of the present proposal, there are two choices of the Kerr medium to be used, to measure the high electric field applied to the target cells. First, a few samples made of a Kerr-material can be placed inside the high voltage electrode system but outside the neutron storage cells. An appropriate Kerr material is acrylic which has a large Kerr constant: $K_A = 3.52 \cdot 10^{-12}$ cm/V^2 measured at room temperature [7].

The second, and much more attractive possibility is to use the superfluid ^{4}He inside the neutron storage cell as the Kerr-active medium. However there is neither experimental nor theoretical published work with data on the Kerr effect in liquid He. Nevertheless a simple estimate of this effect can be performed by using the experimental data available for He gas at room temperature, and by *ab initio* analysis.

In an external electric field E_0, the induced dipole moment of a He atom is

$$P = \alpha E_0 + \gamma E_0^3 / 6 + \ldots,$$

where α is the scalar polarizability, and γ is the hyperpolarizability of the atom. It is γ that gives rise to the Kerr effect [8]. Room-temperature measurements give $\gamma = 44.1 \pm 0.6$ au.[9]. For our estimate we assume that this intrinsic atomic parameter, γ, is independent of temperature, and use this value of γ, the density, and the refractive index of LHe to predict: $K_{LHe} \approx 1.7 \times 10^{-16}$ cm/V^2.

For an electric field of E_0=50 kV/cm applied to a 10 cm long sample of LHe, the induced ellipticity is $\varepsilon = \pi l K E^2 \approx 10^{-5}$ rad. With the polarimeter sensitivity of $\delta\varepsilon \sim 10^{-8}$ rad/s$^{1/2}$, a one second measurement of the electric field, E_0, gives an accuracy of $\delta E_0 / E_0 \approx 5 \times 10^{-4}$. An additional improvement of the sensitivity to the electric field can be achieved using a multipass amplification of the induced ellipticity.

A cryogenic experiment that includes a precise measurement of the Kerr constant of the acrylic (which is considered as a possible material for the neutron storage cells), as well as the Kerr constant of superfluid helium, is in progress at Berkeley.

3. RF coil for spin rotation

The function of the "$\pi/2$" RF coil is to rotate the spin orientation of the polarized ^{3}He and polarized UCNs from the horizontal (*x*) direction to the vertical direction along the *y*-*z* plane. A static uniform magnetic field, B_0, along the *x*-axis will then precess the ^{3}He and the UCNs. In order to accomplish this $\pi/2$ rotation, an RF coil is turned on to generate an oscillating magnetic field, B_{RF}, along the horizontal *z*-axis;

$$B_{RF}(t) = 2B_1 \cos(\omega_{RF} t)\hat{z} \,. \qquad \text{(V.E.5)}$$

Typically, the RF frequency of the coil, ω_{RF}, is tuned to the Larmor frequency of the particle to be rotated, namely, $\omega_{RF} = \gamma B_0$, where γ is the gyromagnetic ratio of the particle. In order to rotate the spin by 90º, the RF field is turned on for a duration, τ, such that $\gamma B_1 \tau = \pi/2$.

For this proposed experiment, the RF coil needs to rotate simultaneously the ^{3}He and the neutron spins, by 90º. Since the gyromagnetic ratio for ^{3}He, γ_3, is ~ 11% higher than the gyromagnetic ratio of the neutron, γ_n, it is not obvious that a suitable RF frequency and pulse duration can be found to accomplish this. In the following we present a numerical solution to this problem.

The linear RF field of Eq. V.E.5 can be expressed in terms of two rotating components:

$$B_{RF}(t) = B_1(-\sin\omega_{RF} t\hat{y} + \cos\omega_{RF} t\hat{z}) + B_1(\sin\omega_{RF} t\hat{y} + \cos\omega_{RF} t\hat{z}) \qquad \text{(V.E.6)}$$

In a frame rotating counterclockwise at ω_{RF} along $\hat{x}$, the first field of Eq. V.E.6 would look static while the other would rotate at $2\omega_{RF}$ for $B_1 << B_0$. The effect of the counter-rotating field at $2\omega_{RF}$ on the spin precession can be safely ignored in the so-called "rotating wave approximation." In this rotating frame, the strength of the static B_0 field appears to be reduced, $B_0 \rightarrow B_0 - \omega_{RF}/\gamma$, according to Larmor's theorem. Therefore, the magnetic field in this rotating frame has two components: the first being the B_1 field along the $\hat{z}'$ axis, and the second being the residual field $B_0 - \omega_{RF}/\gamma$ along the $\hat{x}'$-axis. Note that we use $\hat{x}'$, $\hat{y}'$, $\hat{z}'$

for the rotating frame. The neutron spin will then precess along the direction $B_0 - \omega_{RF} / \gamma_n \hat{x}' + B_1 \hat{z}'$, while the ^{3}He spin will precess along the direction $B_0 - \omega_{RF} / \gamma_3 \hat{x}' + B_1 \hat{z}'$.

Assuming that the neutron's spin is initially along the $\hat{x}$ axis, one can readily obtain the following relation for t, the duration for the RF pulse required to rotate the neutron into the horizontal plane:

$$\cos \omega_n t = -\tan^2 \theta_n . \qquad \text{(V.E.7)}$$

where ω_n is the Larmor frequency of the neutron and θ_n is the angle between direction of the total B field and $\hat{z}'$ for the neutron in the rotating frame:

$$\omega_n = \gamma_n \left[B_1^2 + (B_0 - \omega_{RF} / \gamma_n)^2 \right]^{1/2}$$
$$\tan \theta_n = (B_0 - \omega_{RF} / \gamma_n) / B_1 \qquad \text{(V.E.8)}$$

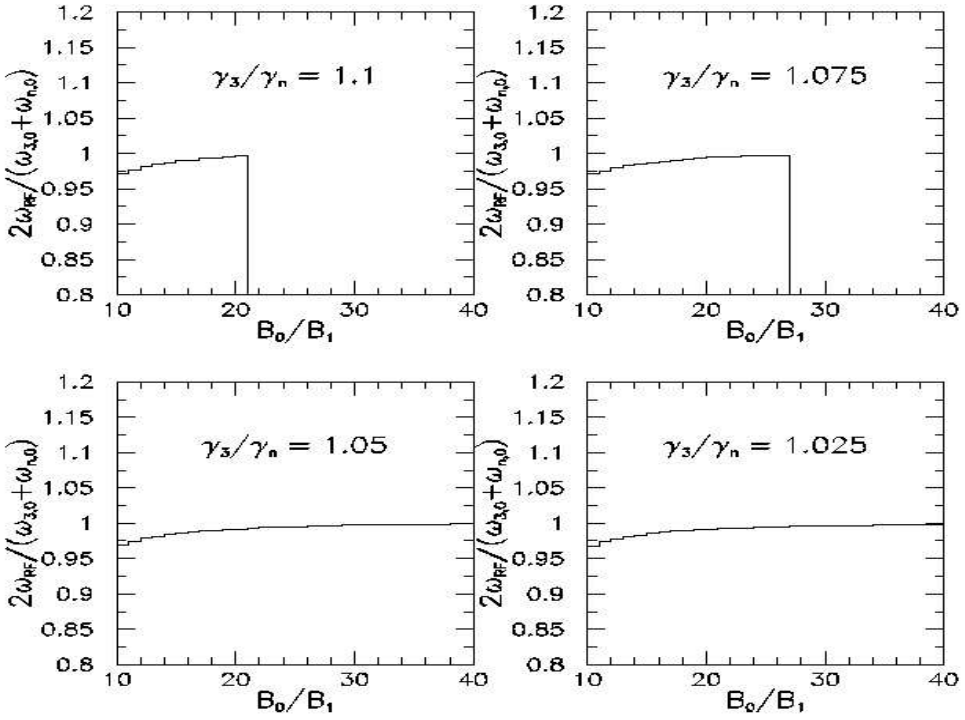

Figure V.E.7. Results of the calculations for ω_{RF} as a function of B_0 / B_1 for various ratios of γ_3 / γ_n.

Expressions analogous to Eqs. V.E.7 and V.E.8 are readily obtained for ^{3}He. The appropriate RF frequency for rotating neutron and ^{3}He spins simultaneously by 90º, can be obtained by solving the following equation:

$$\cos^{-1}(-\tan^2\theta_3) = \frac{\omega_3}{\omega_n}\cos^{-1}(-\tan^2\theta_n). \qquad \text{(V.E.9)}$$

Figure V.E.7 shows the numerical solutions for Eq. V.E.9. $\omega_{3,0} = \gamma_3 B_0$ and $\omega_{n,0} = \gamma_n B_0$ are the Larmor frequencies of the ^{3}He and the neutron in the static B_0 field. For γ_3 / γ_n = 1.1, a solution exists if B_0 / B_1 is less than ~21. Note that $\omega_{RF} \rightarrow \omega_{3,0} + \omega_{n,0}/2$ as B_0 / B_1 increases.

For this proposed experiment, we can select B_0 / B_1 = 20 and $\omega_{RF} = \omega_{3,0} + \omega_{n,0}/2$. Assuming B_0 = 1 mG, this implies that the RF coil will have a magnetic field of $2B_1$ = 0.1 mG with an oscillation frequency of ~3.165 Hz and a duration of ~1.58 seconds.

References

[1] Steve Lamoreaux, *Phy. Rev.* **A53**, 3705 (1996).
[2] Richard Mischke, Report on ANSYS Model Results, February, March, 2002 (http://p25ext.lanl.gov/~mischke/edm/edm_ppt.html).
[3] Handbook of Chemistry and Physics, The Chemical Rubber Co., Section E.
[4] S. Huard, *Polarization of light* (Wiley, New York, 1997).
[5] V. S. Zapasskii and P. P. Feofilov, *Sov. Phys. Uspekhi* **18**(5), 323 (1975).
[6] G. N. Birich, Y. V. Bogdanov, S. I. Kanorskii, I. I. Sobel'man, V. N. Sorokin, I. I. Struk, and E. A. Yukov, *J. of Russian Laser Research* **15**(6), 455 (1994).
[7] T. K. Ishii, A. Griffis, *Microwave and Optical Technology Letters* **4**(10), 387 (1991).
[8] L. W. Bruch, P. J. Fortune, D. H. Berman, *J. Chem. Phys*. **61**(7), 2626 (1974).
[9] S. C. Read, A. D. May, G. D. Sheldon, *Can. J. Phys*. **75**(4), 211 (1997).

Chapter V.E Appendix

High Voltage Considerations

It is important to utilize the maximum electric field achievable in the EDM experiment. Previous experiments have used a field of typically 1 KV/mm. The design goal for this experiment is 5 KV/mm. The feasibility of this goal has been investigated by searching the literature for information on the dielectric strength of liquid Helium. Several measurements have been reported, but typically these are for very small gaps between electrodes. There are no data that match the requirements for this experiment. A reasonable summary of existing data is shown in Fig. V.E.6, which is taken from a paper by J. Gerhold [1].

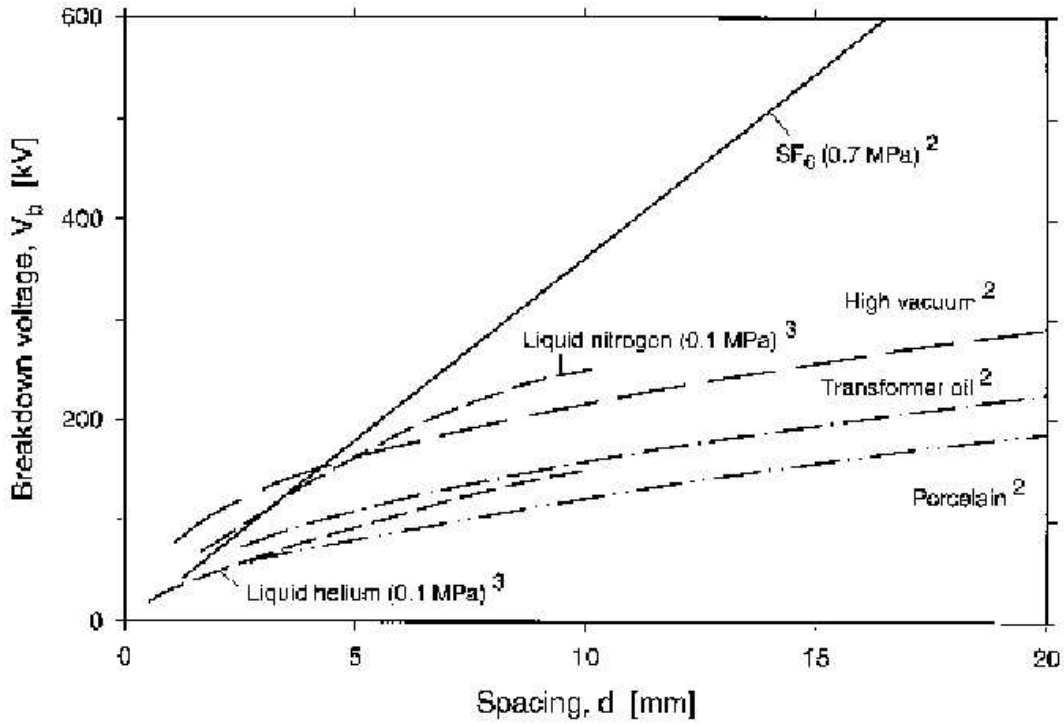

Figure V.E.6 Breakdown strength of typical solid, cryogenic liquids, and vacuum insulation under D.C. voltage stress in a uniform field.

For very small gaps (under 1 mm), the quoted breakdown strength of LHe is impressive: ~70 KV/mm[2]. However, as seen in Fig. V.E.6, the breakdown strength is only 15 KV/mm for a 1 cm gap. The suggested guidance for extrapolation to larger gaps (*d*) is that the breakdown voltage is proportional to $\sqrt{d}$. This implies a value of ~5 KV/mm for a gap of 10 cm, which gives a very small margin of safety for this experiment. Unfortunately, there are additional factors that degrade the breakdown limit. Two of these are time and volume. The measured dependencies from Ref. 1 are shown in Figs. V.E.7 and V.E.8. Again, for this experiment, huge extrapolations are required. The volume in Fig. V.E.7 extends to 10^5 mm^3 while the volume needed is $2x10^7$ mm^3.

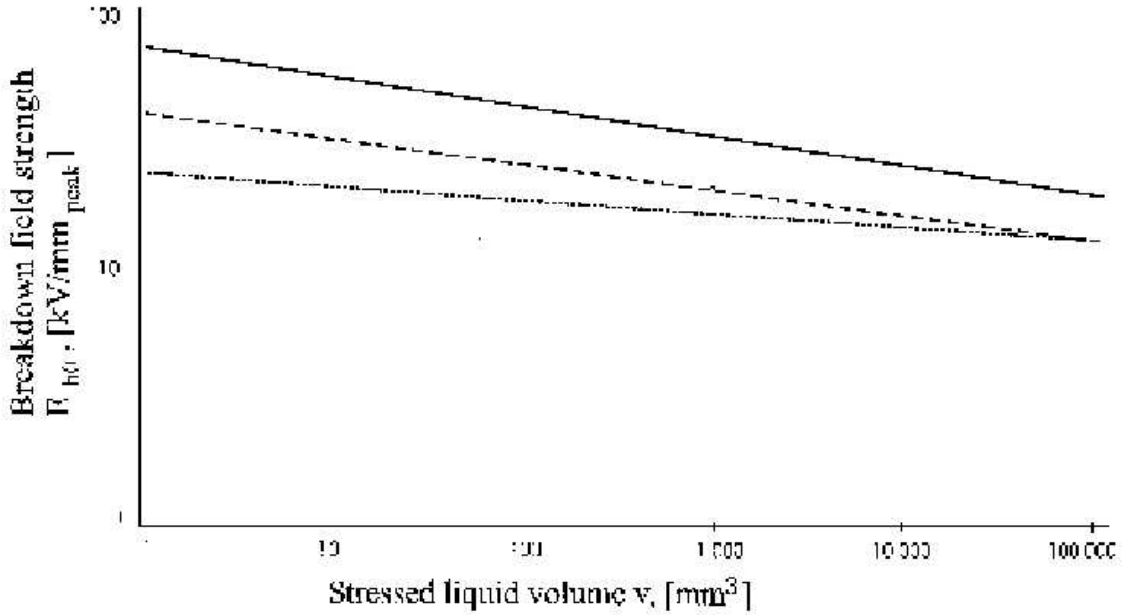

Figure V.E.7. Volume effect in liquid helium breakdown. The lowest line is "near zero breakdown probability."

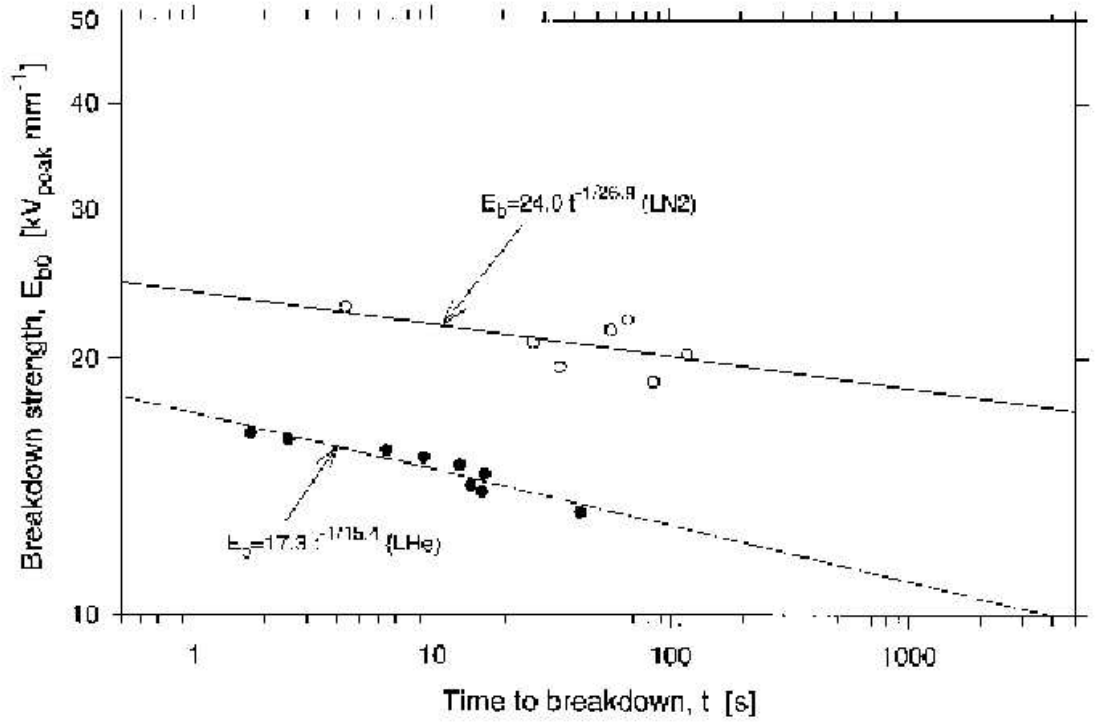

Figure V.E.8. Breakdown strength-time characteristics at power frequency in a coaxial cylindrical electrode system; spacing 4.5 mm, cylinder diameter 42.5 mm and length 100 mm.

The data for time to breakdown in Fig. V.E.8 extends to ~100 s while the requirement here is for no breakdowns for the duration of the experiment, or ~10^8 s because of possible damage to the SQUIDS from a spark.

Naïve extrapolation would lead to predictions for a breakdown strength below that desired for the experiment. However, there is reason for optimism, as Gerhold says that "distinct experimental data are scarce at present, but LHe breakdown much below ~10 KV/mm has never been reported."[3] Because of the importance of this topic for the expectations of the experiment and the risks of extrapolation, it is essential that the breakdown strength in LHe be measured directly for the conditions of this experiment.

Another potential issue is the difference in breakdown strength between normal and superfluid He. The measurements displayed in Figs. 1-3 are for normal LHe. In Fig. V.E.9, the breakdown strength for superfluid He is shown [1]. For a gap of 1 mm, the breakdown strength is a factor of 2 below that of normal LHe, but again the behavior for large gaps has not been measured.

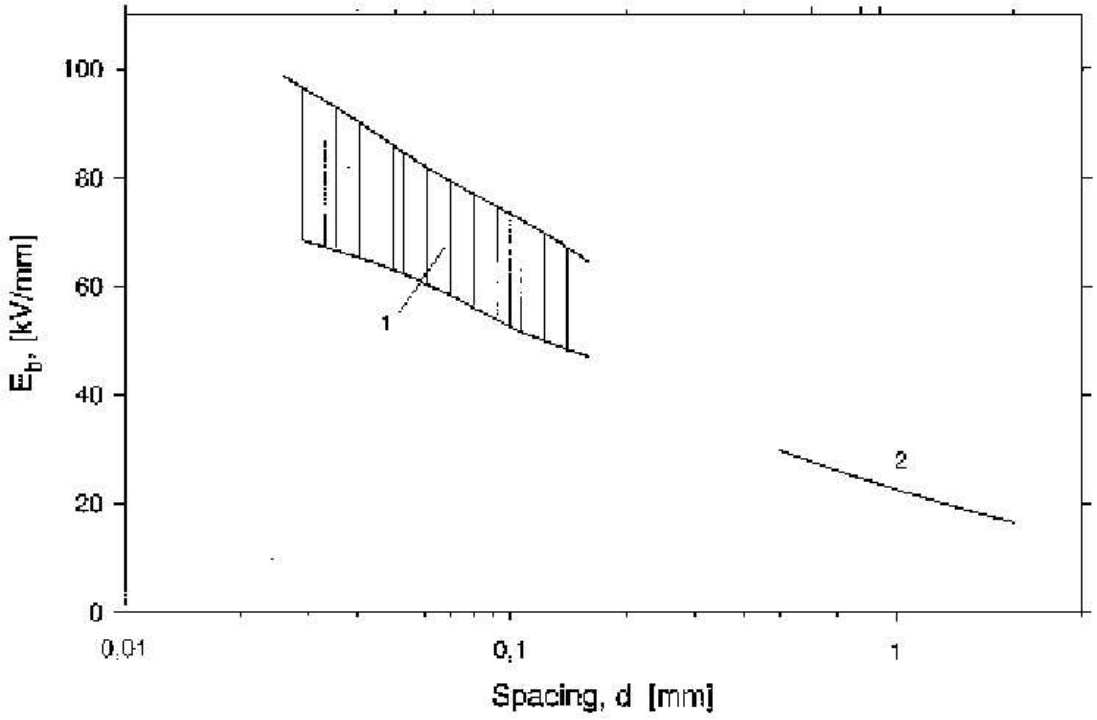

Figure V.E.9. Uniform field DC breakdown strength of saturated LHe II near 2.0 K vs spacing.

References:

[1] J. Gerhold, *Cryogenics* **38**, 1063 (1998).

[2] B.S. Blaisse et al., *Bull. Inst. Int. Froid, Suppl*., 333 (1958).

[3] J. Gerhold, IEEE Trans. on *Dielectrics and Electrical Insulation* **5**, 321 (1998).